

# A Knowledge-Based Approach for Carpal Tunnel Segmentation from Magnetic Resonance Images

Hsin-Chen Chen · Yi-Ying Wang · Cheng-Hsien Lin ·  
Chien-Kuo Wang · I-Ming Jou · Fong-Chin Su ·  
Yung-Nien Sun

Published online: 9 October 2012  
© Society for Imaging Informatics in Medicine 2012

**Abstract** Carpal tunnel syndrome (CTS) has been reported as one of the most common peripheral neuropathies. Carpal tunnel segmentation from magnetic resonance (MR) images is important for the evaluation of CTS. To date, manual segmentation, which is time-consuming and operator dependent, remains the most common approach for the analysis of the carpal tunnel structure. Therefore, we propose a new knowledge-based method for automatic segmentation of the carpal tunnel from MR images. The proposed method first requires the segmentation of the carpal tunnel from the most proximally cross-sectional image. Three anatomical features of the carpal tunnel are detected by watershed and polygonal curve fitting algorithms to automatically initialize a deformable

model as close to the carpal tunnel in the given image as possible. The model subsequently deforms toward the tunnel boundary based on image intensity information, shape bending degree, and the geometry constraints of the carpal tunnel. After the deformation process, the carpal tunnel in the most proximal image is segmented and subsequently applied to a contour propagation step to extract the tunnel contours sequentially from the remaining cross-sectional images. MR volumes from 15 subjects were included in the validation experiments. Compared with the ground truth of two experts, our method showed good agreement on tunnel segmentations by an average margin of error within 1 mm and dice similarity coefficient above 0.9.

---

H.-C. Chen · Y.-N. Sun  
Department of Computer Science and Information Engineering,  
National Cheng Kung University,  
No. 1, University Road,  
Tainan 701, Taiwan, Republic of China

H.-C. Chen  
e-mail: hsinlovehsin@gmail.com

Y.-Y. Wang  
Hermes Microvision Inc.,  
7F., No.18, Puding Rd., East Dist.,  
Hsinchu City 300, Taiwan, Republic of China  
email: yiying999@gmail.com

C.-H. Lin  
Flight Testing Division, Chung-Shan Institute of Science  
and Technology,  
Longtan, Taiwan, Republic of China  
email: chlin0609@gmail.com

C.-K. Wang  
Department of Radiology, National Cheng Kung University  
Hospital,  
No. 138, Sheng Li Road,  
Tainan 704, Taiwan, Republic of China  
email: n044206@mail.hosp.ncku.edu.tw

I.-M. Jou  
Department of Orthopedics, College of Medicine, National Cheng  
Kung University,  
No. 138, Sheng Li Road,  
Tainan 704, Taiwan, Republic of China  
email: jming@mail.ncku.edu.tw

F.-C. Su  
Institute of Biomedical Engineering, National Cheng Kung  
University,  
No. 1, University Road,  
Tainan 701, Taiwan, Republic of China  
email: fcsu@mail.ncku.edu.tw

H.-C. Chen · I.-M. Jou · F.-C. Su · Y.-N. Sun (✉)  
Medical Device Innovation Center, National Cheng Kung  
University,  
Tainan, Taiwan, Republic of China  
e-mail: ynsun@mail.ncku.edu.tw

**Keywords** Carpal tunnel · Knowledge-based segmentation · MR · Deformable model · Watershed · Polygonal curve

## Introduction

The carpal tunnel is a passageway in the wrist, formed by the carpal bones and the transverse carpal ligament. The carpal tunnel encloses a median nerve and nine digit flexor tendons passing from the forearm into the hand. These tissues are essential for performing normal hand functions. When the median nerve becomes compressed, squeezed, or irritated, carpal tunnel syndrome (CTS), which is the most frequent compressive neuropathy in the upper extremity, will occur. CTS is progressive and produces numbness, pain, swelling, and weakness of hands, causing significant inconvenience for patients. The prevalence of CTS has been reported from 1 to 3 % in a general population [1], and there is some evidence indicating that the incidence of CTS is increasing [2]. Moreover, about 400,000 procedures of carpal tunnel release, which is the most common hand and wrist surgery, are performed in the USA per year [2]. Although CTS has been shown to be a compression neuropathy convincingly, how the compression is generated or maintained have not been identified definitely [3, 4]. Investigation into causes and pathologies of CTS hence becomes a critical issue.

In recent years, a lot of progress has been made in noninvasive imaging methods, such as magnetic resonance (MR) imaging. It has been reported that the MR imaging technique is able to accurately and reliably visualize the three-dimensional (3D) geometries of the carpal tunnel and some of its contents to quantitatively measure the carpal tunnel [5, 6]. Ablove et al. [7] estimated the morphological changes in the carpal tunnel before and after carpal tunnel release surgery using MR images. In addition, Cobb et al. [8] performed a preliminary study that assessed the ratio of carpal contents to carpal tunnel volume in patients with CTS. Uchiyama et al. [9] investigated the correlation between the severity of CTS and the geometry features of the carpal tunnel (e.g., palmar bowing of the transverse carpal ligament) using MR images. More recently, Mogk and Keir [10, 11] evaluated the shape and size of the carpal tunnel in different wrist postures based on MR images. Pacek et al. [4] investigated the correlation between carpal tunnel and hand dimensions based on a morphological analysis of the carpal tunnel. From the above-mentioned literature, it can be posited that the quantitative measurements of the carpal tunnel from MR images are essential for investigating structural changes associated with CTS. However, all of them have adopted the manually segmentation approach for estimating their target measurements. Thus, their measuring process is tedious and time-consuming, and moreover, the resulting measurements are not reproducible due to intra- and interoperator variability.

Because segmentation results greatly influence measurement accuracy, segmentation is the most critical step of carpal tunnel measurement. Changes in carpal tunnel pressure, which behave as a function of tunnel volume as well as the volume of its contents, could be detected based on the segmentation results and are important signs of tunnel compression [10]. However, the median nerve usually presents unclear and inconsistent intensity appearance in MR images, making automatic nerve segmentation challenging. Changes in spatial configuration of carpal tunnel and flexor tendons potentially provide insight into median nerve trauma [12–14], so the present study focuses on the automatic segmentation of tunnel and tendons, rather than directly segments and analyzes the morphology of median nerve. Although there have been a large number of studies dedicated to the design of segmentation methods for different modalities of medical images, the work of Kunze et al. [15] is the only one that has been found to be related to automatic analysis of carpal tunnel MR images. Kunze presented a region-based method to semiautomatically segment the flexor tendons, while the boundary of the carpal tunnel was still identified manually. For this purpose, our research aims to develop an image analysis system for automatic segmentation and quantitative measurement of carpal tunnel.

In the past, region-based methods [16–18] have been extensively developed to address the issue of image segmentation. Two typical methods are the watershed [16] and region growing [17] methods. Region-based methods can delineate regions with homogeneously distributed intensities well. However, their performance depends on the intensity gradient strength of the target boundary. A severe edge-leaking problem tends to occur when the intensity gradient is weak, which is often seen in carpal tunnel segmentation. Purely region-based methods are thus unsuitable for carpal tunnel segmentation in the present study.

To overcome this problem, deformable model (DM)-based segmentation methods [19–23] have been developed. Two typical deformable models are the active contour model (snakes) [19] and the active shape model [21]. Such methods usually achieve segmentation by adjusting the deformable model to the strong edges of a target object. As the deformation process refers to not only the intensity information of the image but also the bending degree of the model shape, DM-based methods can usually avoid significant segmentation errors even when the boundaries of the target object are vague. In these methods, the initial position and shape of the DM are major concerns. Convergence to the true solution is very likely to fail if the distance between the contours of the target object and the DM is too large.

Recently, DM-based approaches incorporating anatomical knowledge have been developed to handle this problem. Han et al. [24] proposed a coarse-to-fine strategy with hand

anatomy knowledge for epiphyseal region segmentation. They first utilized the watershed approach to extract hand bones and then determined the location of the initial epiphyseal model based on the bone positions. Seifert et al. [25] presented a segmentation method for the soft tissues of the cervical spine based on spine anatomy. This issue was also addressed by Yu et al. [26] for fetal ultrasound image segmentation. These methods combined anatomical knowledge with segmentation protocols in order to initialize the model closely to the target and increase the accuracy of the segmentation.

Nevertheless, there are still some difficulties with segmenting MR carpal tunnel images that were not resolved in these studies. For instance, several edges of irrelevant tissues, including carpal bones, ligaments, and flexor tendons, are located nearby the tunnel. Such a complex context may make segmentation unstable. Meanwhile, the boundary of carpal tunnel is usually vague due to the partial volume effects of MR imaging, thus perplexing the definition of the tunnel boundary. In addition, the tunnel position, shape, and boundary appearance have large variations among different cross-sectional images and thus increase the complexity of segmentation procedures. In general, a 3D DM approach is a more natural choice to segment a 3D structure. However, the above-mentioned difficulties make it impractical to automatically initialize a suitable 3D tunnel model close to the true tunnel surface. Reliable segmentation is thus rarely a result using a fully 3D approach.

In this paper, we propose a new 2D knowledge-based method for carpal tunnel segmentation in MR images. The proposed method incorporates anatomical knowledge of carpal tunnel with object segmentation algorithms to overcome the aforementioned difficulties. The major features of the proposed method are described below. Two algorithms based on watershed and polygonal curve fitting are designed to detect the anatomical features of the carpal tunnel. By means of the geometrical information from the detected features, we are able to automatically initialize a DM close to the carpal tunnel in the MR image and properly constrain the geometry of the DM in the segmentation process. Moreover, the intensity properties of MR images and geometry information about the tunnel and its contents are jointly utilized for the purpose of capturing the true boundary of the carpal tunnel in the MR image. Furthermore, a sequential contour propagation strategy is designed to compensate the shape changes in the carpal tunnel in adjacent images caused by interslice gaps. Finally, our proposed method does not need user interventions in the carpal tunnel segmentation process, thus avoiding intra- and interoperator variability. The rest of this paper is organized as follows: the image acquisition and description, the details of the proposed segmentation method, the experimental results, the discussion, and finally the conclusions.

## Image Acquisition and Description

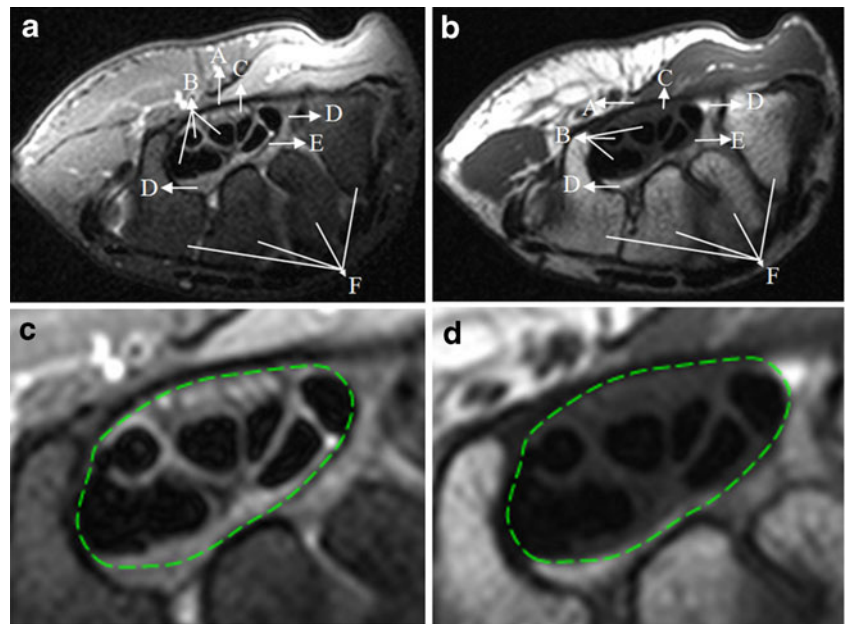
This study was approved by National Cheng Kung University Hospital Institutional Review Board, and participants gave informed consent. All MRI examinations in the following experiments were performed using the same 1.5-T whole-body MR imaging system (Achieva; Philips Medical Systems, Best, The Netherlands) with a phased-array surface coil placed on the palmar aspect of the affected wrist with the patient in an MR imager. Imaging sequences include the following: an axial spin-echo T1-weighted sequence (repetition time ms/echo time ms 500–682/15–18; flip angle, 90°) and axial spin-echo intermediate-weighted (i.e., PD-weighted) sequence (2,000–3,000/15–30; flip angle, 90°; echo train length, 5; and spectral fat saturation) with two excitations. All MRI examinations with 22 contiguous slices were performed with a field of view of 10 cm, a matrix size of 200×198, and a slice thickness of 2 mm with no interslice gap. The imaging region covers from distal radius to carpometacarpal joint, which was under the supervision of the radiologist (Chien-Kuo Wang).

Figure 1 shows examples of the MR images acquired from PD (Fig. 1a) and T1 (Fig. 1b) scans. Through joint reference to both images, we are able to delineate the boundary of the carpal tunnel, which is surrounded by the transverse carpal ligament and deep fascia, as shown in Fig. 1c and d. The tunnel can also be thought of as a passageway that is formed by the transverse carpal ligament and carpal bones without including the fatty tissues. The intensity contrast between the transverse carpal ligament and its surrounding regions in PD images is greater than that in T1 images. Moreover, the fatty tissues show much higher intensity in T1 images than in PD images. Using either a PD or a T1 scan is insufficient for featuring the intensities of all tissues adjacent to the carpal tunnel and demarcating the carpal tunnel from the wrist structure. To obtain sufficient information for carpal tunnel segmentation, both PD and T1 images are used in the proposed method. In the rest of this paper, PD and T1 images are denoted as  $I_{PD,c}$  and  $I_{T1,c}$ , respectively, where  $c=1, 2, \dots, N-1, N$ , is the index of the cross-sectional images along the distal-proximal direction, and  $N$  is the number of the cross-sectional images.

## Method

The anatomical context around the carpal tunnel is very complex, as shown in Fig. 1, making it difficult to automatically separate the tunnel solely based on intensity. In order to handle such a problem, we design a new knowledge-based segmentation protocol by utilizing anatomical knowledge of carpal tunnel on the cross-sectional images. Three anatomical features, including the digit flexor tendons, the transverse carpal ligament, and deep fascia, are used to

**Fig. 1** Examples of two corresponding cross-sectional images: **a** the PD-weighted image, **b** the T1-weighted image. *A* transverse carpal ligament, *B* digit flexor tendons, *C* median nerve, *D* fat, *E* deep fascia, *F* carpal bones. **c**, **d** The boundary of the carpal tunnel shown on the enlarged subregions of **a** and **b**, respectively



identify the tunnel border position and to construct an approximate model of the carpal tunnel for achieving subsequent stable and accurate segmentation. Based on anatomical knowledge, the tunnel structures are progressively segmented from the proximal side toward the distal direction to obtain the complete carpal tunnel structure.

The tendons, located inside the tunnel, are first detected from the most proximally cross-sectional image, and the detection results are then applied to delineate the ligament and deep fascia, which are parts of the carpal tunnel boundary. Using the three detected features, a DM with a proper initial shape and position for the carpal tunnel can be generated and subsequently fitted to the image in order to segment the carpal tunnel. Considering that the anatomical structures in the adjacent cross-sectional images are similar in shape, we then design a sequential contour propagation strategy to segment the remaining images. Lastly, a 3D carpal tunnel can be reconstructed from a stack of segmented cross-sectional images.

### Carpal Tunnel Feature Detection

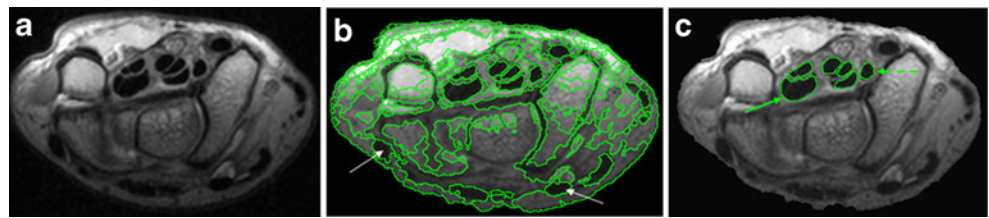
#### *Digit Flexor Tendons*

The proposed method employs the morphological watershed [16] to extract the regions of the digit flexor tendons within the carpal tunnel in the most proximally cross-sectional image. Generally, uniformly distributed intensities in the target regions and a high degree of contrast intensity with regard to the surrounding regions are helpful for achieving a stable segmentation process. We hence average  $I_{PD, N}$  and  $I_{T1, N}$  and then obtain the average image  $\overline{I_N}$  (see Fig. 2a). The average image

maintains uniformly low intensities inside the tendon regions, a large intensity difference between the tendons and the bones, and a high intensity contrast between the tendons and their surrounding regions. Thus, it is used as the input image of the watershed.

After the watershed segmentation, a large number of homogeneous regions including tendons and nontendons can be obtained, as shown in Fig. 2b. As can be seen in Fig. 2a, the tendons are dark in intensity, circular in shape, and have sizes in a certain range. A region, which has geometry and intensity properties dissimilar to those of tendons, is then removed when one of the following rules is satisfied: (1) the area is too large (i.e., the number of pixels is more than 2,000 pixels) or too small (i.e., the number of pixels is less than 50 pixels); (2) the brightness is not low (i.e., the intensity is larger than 50); (3) the shape is non-circular (i.e., the longitudinal length is larger than 40 pixels [27]). After that, there are still a few regions that are similar in appearance to the tendons but not enclosed by the carpal tunnel, as indicated by the arrows in Fig. 2b. Considering that the flexor tendons inside the tunnel are located close together because of the constraints of tunnel geometry, we subsequently utilize our previously developed distance-based grouping approach [28] to pick out those target tendons within the carpal tunnel. Consequently, the digit flexor tendons in the most proximally cross-sectional image can be obtained (see Fig. 2c) and denoted as  $TD_N$ . The solid and dashed arrows in Fig. 2c indicate the ulnar- and radial-side end points, respectively. Based on  $TD_N$ , the flexor tendons in the other cross-sectional images, i.e.,  $TD_1, TD_2, \dots, TD_{N-1}$ , can subsequently be detected using a registration-based segmentation approach [28].

**Fig. 2** Digit flexor tendon detection: **a** the PD-T1 average image, **b** the result of watershed flooding, and **c** the result of digit flexor tendon detection



### Transverse Carpal Ligament and Deep Fascia

The transverse carpal ligament and deep fascia are of great importance in estimating the border positions of the carpal tunnel. Anatomical knowledge about their shape is utilized in the detection process. Since their shape is limited in the degree of bending, a two-segment polygonal curve is used to approximate their shape and position. In addition, their intensity contrast relative to the neighboring regions in PD images is greater than that in T1 images. We thus design a polygonal curve fitting algorithm to detect the ligament and deep fascia from  $I_{PD, N}$ .

The polygonal curve used in the proposed method consists of two line segments, which are specified by three consecutive control points  $\mathbf{p}_1$ ,  $\mathbf{p}_2$ , and  $\mathbf{p}_3$ . By rotating  $\mathbf{p}_2$  and  $\mathbf{p}_3$  around  $\mathbf{p}_1$  by angle  $\theta$  and translating  $\mathbf{p}_1$ ,  $\mathbf{p}_2$ , and  $\mathbf{p}_3$  by vector  $\mathbf{t}$ , we are able to globally adjust the orientation and position of the curve, as shown in Fig. 3a and b, respectively. The dashed and solid curves indicate the curves before and after adjustment, respectively. Moreover, we are able to adjust the local shape of the curve by moving  $\mathbf{p}_2$  with vector  $\mathbf{d}$  (see Fig. 3c), which determines the position and height of the curve's peak. By adjusting pose parameters  $\theta$ ,  $\mathbf{t}$ , and  $\mathbf{d}$ , a specific pose of the polygonal curve can then be obtained.

Now that we have specified the structure of the polygonal curve, we next describe the feature detection process. We first generate a polygonal curve for the transverse carpal ligament with an initial pose indicated by the dashed line in Fig. 3d. The control points  $\mathbf{p}_1$  and  $\mathbf{p}_3$  are placed at the ulnar- and radial-side end points of the tendon regions, respectively, and  $\mathbf{p}_2$  is given as the intermediate point between  $\mathbf{p}_1$  and  $\mathbf{p}_3$ . With the initial polygonal curve, the ligament, which is a thick band with low

intensity in axial images, can then be estimated by finding the pose parameters that maintain the minimal sum of intensity on the curve. In addition, we first generate a polygonal curve with the same initial pose for the detection of the deep fascia of the carpal tunnel. The deep fascia, which lies in the transition from bright to dark regions, is then found by solving the optimal pose parameters, which maintain the maximal sum of directed pose gradient strength on the curve.

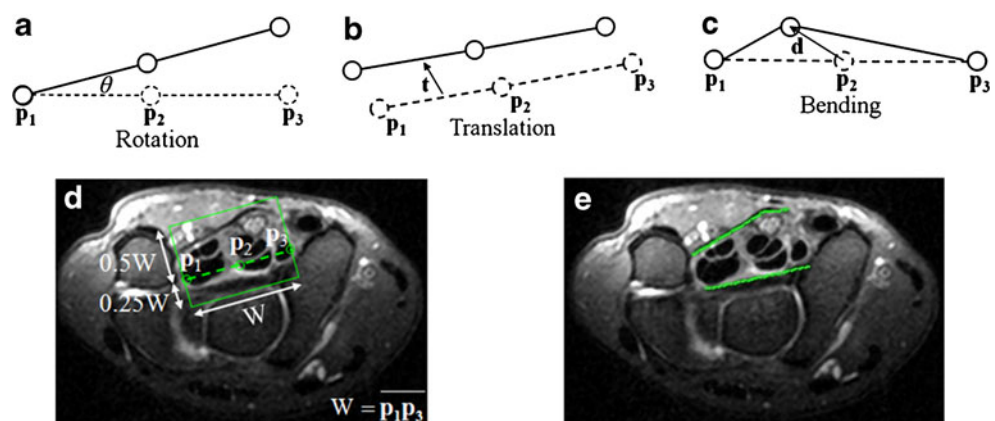
In the implementation, a geometrical condition based on the anatomy of a carpal tunnel is taken into account in order to reduce the computation time of the optimization process. The tunnel is elliptical shaped in the axial view and therefore is supposed to be enclosed by a rectangle. Based upon such prior knowledge, the search space for the optimal polygonal curves can be confined to a smaller range, instead of the entire image, as indicated by the rectangle in Fig. 3d. In our experiments, the major axis of the rectangle was parallel to the direction from the ulnar- to radial-side end points of the tendon regions. The length of the long side was specified as the distance between the two end points, and the length of the short side was set to three fourths the length of the long side. After solving the pose parameters of the two polygonal curves, the transverse carpal ligament and deep fascia could be detected, as indicated by the solid curves in Fig. 3e.

### Carpal Tunnel Segmentation

#### Deformable Model Initialization

Given the spatial information of carpal tunnel features, the initial shape and position of the DM can then be determined. We connect the ulnar-side end point of the tendon regions to

**Fig. 3** Transverse carpal ligament and deep fascia detection: **a–c** pose adjustment of the curve by rotation, translation, and bending, respectively; **d** the initial polygonal curve and solution search space; and **e** the detection results of the transverse carpal ligament (top) and deep fascia (bottom) shown in the PD-weighted image



the ulnar-side end points of the ligament and deep fascia. Similarly, the radial-side end point of the tendon regions can be connected to the radial-side end points of the ligament and deep fascia. Consequently, a closed contour (see Fig. 4a) near to the boundary of the carpal tunnel of the underlying image can be automatically obtained as the initialized DM.

*Energy Function of the Deformable Model*

To obtain a good fit between the DM and the underlying image, the initial contour of the DM is deformed toward the true boundary of the carpal tunnel via minimizing energy function  $E_{total}$ :

$$E_{total} = \sum_{i=1}^M [wE_{edge}(\mathbf{v}_i) + (1 - w)E_{shape}(\mathbf{v}_i) + C_{geometry}(\mathbf{v}_i)] \tag{1}$$

where  $E_{edge}$  is the edge energy,  $E_{shape}$  is the shape energy, and  $C_{geometry}$  is the geometry constraint.  $\mathbf{v}_i$  represents the coordinate of the  $i$ th point of the DM,  $M$  is the number of model points, and  $w$  is a weighting value. The edge energy measures the boundary fitness between the DM and the underlying image. The boundary of the carpal tunnel is expected to appear in the transition from high to low intensity (i.e., from inside tunnel toward outside) in the PD scan. Moreover, based on anatomical knowledge in delineating the carpal tunnel, the tunnel region should exclude the fatty tissues, which are characterized by high-intensity signals in the T1 scan and usually adjoin the tunnel as shown in Fig. 1. To characterize such intensity properties of the carpal tunnel in the segmentation process, we design  $E_{edge}$  based on the intensity information from both T1 and PD images:

$$E_{edge}(\mathbf{v}_i) = \sum_{j=1}^{j=3} \varphi(\mathbf{v}_i + j\mathbf{n}(\mathbf{v}_i)) - \sum_{j=-3}^{j=-1} \varphi(\mathbf{v}_i + j\mathbf{n}(\mathbf{v}_i)), \tag{2}$$

$$\varphi(\mathbf{x}) = \begin{cases} \frac{1}{3}I_{PD,c}(\mathbf{x}), & \text{if } I_{T1,c}(\mathbf{x}) > I_f \\ I_{PD,c}(\mathbf{x}), & \text{otherwise} \end{cases}$$

where  $\mathbf{n}(\mathbf{v}_i)$  denotes the outward-pointing normal vector of model contour at  $\mathbf{v}_i$ ,  $c$  is the index of the cross-sectional images,  $I_f$  is a threshold value indicating the fatty tissues, and  $\varphi$  is an intensity transform function. If a pixel in  $I_{T1, c}$

has an intensity signal higher than  $I_f$ , then its intensity in  $I_{PD, c}$  is reduced to sharpen the changes of intensity near the carpal tunnel boundary. In other words, the evidence of the carpal tunnel boundary can be reinforced using the proposed edge energy.

The shape energy indicating the contour curvature of the DM is defined as

$$E_{shape}(\mathbf{v}_i) = \|\mathbf{v}_{i+1} + \mathbf{v}_{i-1} - 2\mathbf{v}_i\| \tag{3}$$

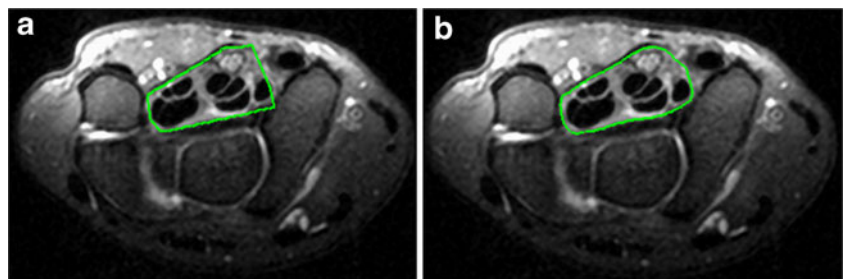
where  $\mathbf{v}_{i-1}$ ,  $\mathbf{v}_i$ , and  $\mathbf{v}_{i+1}$  are the coordinates of the  $(i-1)$ th,  $i$ th and  $(i+1)$ th points on the DM, respectively. This energy is used to maintain the smoothness of the model shape in the deformation process. On the other hand, the geometry constraint  $C_{geometry}$ , which constrains the movement of points on the DM, is designed based on the geometry relationship between the carpal tunnel and the digit flexor tendons:

$$C_{geometry}(\mathbf{v}_i) = \kappa \cdot |\{\mathbf{v}_i + \delta \cdot \mathbf{n}(\mathbf{v}_i), \delta = 1, \dots, L\} \cap \mathbf{TD}_c| \tag{4}$$

where  $\kappa$  is a large positive constant,  $L$  is the length of the search line, and  $\mathbf{TD}_c$  represents the pixels of the tendon regions in the  $c$ th cross-sectional image. From an anatomical point of view, the digit flexor tendons are completely enclosed by the carpal tunnel contour. Equation 4 is used to maintain such an anatomical condition in the segmentation process; if there are tendon regions excluded from the DM,  $E_{total}$  will be penalized by a large  $C_{geometry}$ . After minimizing  $E_{total}$ , the carpal tunnel of the  $N$ th cross-sectional image can be segmented as shown in Fig. 4b. Compared to the initial contour in Fig. 4a, better boundary fitness between the DM and the carpal tunnel image can be achieved after the contour optimization process.

Equation 1 is minimized by iteratively adjusting the positions of contour points of the DM to fit the true tunnel boundary along the normal directions of points. The iteration converges and stops when the sum of the displacements of vertices between the previous and current iterations is less than two pixels or if the number of iteration reaches 50. On the other hand, the DM's behavior can be controlled by adjusting the system parameters of Eq. 1. In our experiments, they were empirically assigned; the value of  $w$  was set to 0.3. The value of  $\kappa$  was assigned with 1,000, and the value of  $L$  was 13. The value of  $I_f$  was determined by two standard deviations from the mean intensity of the second

**Fig. 4** Carpal tunnel segmentation: **a** initialized DM and **b** the segmentation result for the carpal tunnel shown on  $I_{PD, N}$



highest cluster, which is obtained by applying the  $K$ -means clustering approach ( $K=4$ ) to the T1 images [29].

### Sequential Contour Propagation

In this section, we present a contour propagation strategy, which sequentially matches the segmented tunnel to its adjacent image along the proximal to distal direction in order to achieve the segmentation of the entire MR carpal tunnel volume. In the matching process, given an image pair of  $I_{PD, c}$  and  $I_{PD, c-1}$ , we first align the segmented tunnel of  $I_{PD, c}$  to  $I_{PD, c-1}$  by employing the iterative closest point (ICP) algorithm [30] and then improve the boundary fitness between the aligned tunnel contour and the underlying image through the proposed contour deformation method. The sequential propagation process begins with the most proximally cross-sectional image and finally stops at the most distal image.

Since the longitudinal direction of the carpal tunnel is usually not perpendicular to the MR imaging plane (i.e., axial plane), there is a certain positional offset of the carpal tunnel between  $I_{PD, c}$  and  $I_{PD, c-1}$ . In the proposed method, we utilize the ICP to reduce the spatial offset. The ICP alignment is achieved by iteratively finding a rigid transformation  $\mathbf{RT}$ , which includes a 2D rotation matrix and a translation vector, to minimize the distance of the tendon regions between  $I_{PD, c}$  and  $I_{PD, c-1}$ :

$$Dis(\mathbf{RT}) = \sum_{i=1}^{i=U} \|\mathbf{RT}(\mathbf{p}_i(\mathbf{TD}_c)) - \mathbf{p}_j(\mathbf{TD}_{c-1})\| \quad (5)$$

where  $\mathbf{TD}_c$  and  $\mathbf{TD}_{c-1}$  are the sets of pixels of the tendon regions in the  $c$ th and  $(c-1)$ th cross-sectional images, respectively, which are extracted in the previous section.  $\mathbf{p}_i(\mathbf{TD}_c)$  represents the  $i$ th contour point of  $\mathbf{TD}_c$ , and  $\mathbf{p}_j(\mathbf{TD}_{c-1})$  is the  $j$ th contour point of  $\mathbf{TD}_{c-1}$  that is the closest to  $\mathbf{p}_i(\mathbf{TD}_c)$ .  $U$  is the number of contour points of  $\mathbf{TD}_c$ . The details of numerical computation in optimizing Eq. 5 can be found in [30]. Having the solved transformation  $\mathbf{RT}$ , we are able to map the segmented carpal tunnel in the  $c$ th cross-sectional image to the position, which is close to the tunnel in the  $(c-1)$ th image. The transformed contour then serves as the initial DM, and its shape is subsequently improved through the contour optimization method in the previous section with a reduced search line length ( $L=6$ ). The improved contour consequently serves as the segmentation result of the carpal tunnel in the distally adjacent image. By adopting the proposed contour propagation strategy, which takes the spatial relationship between adjacent frames into account, we can properly maintain the smoothness between the segmentations of two adjacent frames. After the entire propagation process is finished, a stack of segmented cross-sectional images can be obtained for the reconstruction of the 3D carpal tunnel.

## Experimental Results

In the following experiments, the proposed segmentation method was validated with respect to accuracy and reliability using the MR volumes of 15 subjects in the neutral posture. In addition, a comparative study with two other segmentation methods was carried out to show how the proposed ideas could improve segmentation results. For each volume data, the carpal tunnel was automatically segmented using the proposed method.

### Qualitative Assessment

A qualitative evaluation was performed by visually inspecting how well the automatic results were fitted to the true boundary of the carpal tunnel. Figure 5 shows the segmentation results of the carpal tunnel from the validation data. The first and second rows demonstrate the resulting carpal tunnel contours superimposed onto the axial PD images. The surfaces of the segmented carpal tunnels from two subjects were triangulated using the marching cube algorithm [31] and displayed in the third row of Fig. 5.

### Quantitative Evaluation

In addition to the qualitative assessment, the accuracy of the proposed method was also validated by quantitatively comparing the automatic results to the average of the manual results of two experts, which served as the ground truth. For each axial image, a spatial overlap index called the dice similarity coefficient (DSC) [32] and two distance measures including the mean error (ME) and the root mean square error (RMSE) were utilized to evaluate consistency between the automatic result and the ground truth. The three metrics were defined below:

$$DSC = \frac{2|\mathbf{A} \cap \mathbf{B}|}{|\mathbf{A}| + |\mathbf{B}|}, \quad (6)$$

$$ME = \sum_{i=1}^H \sqrt{(\mathbf{u}_i - \mathbf{y}_j)^2} / H, \quad (7)$$

$$RMSE = \sqrt{\sum_{i=1}^H (\mathbf{u}_i - \mathbf{y}_j)^2} / H \quad (8)$$

where  $\mathbf{A}$  and  $\mathbf{B}$  are the sets of pixels of automatic result and ground truth, respectively.  $\mathbf{u}_i$  represents the coordinate of the  $i$ th contour point of the automatic result, and  $\mathbf{y}_j$  is the coordinate of the  $j$ th contour point of the ground truth, which is the closest to  $\mathbf{u}_i$ .  $H$  is the number of contour points

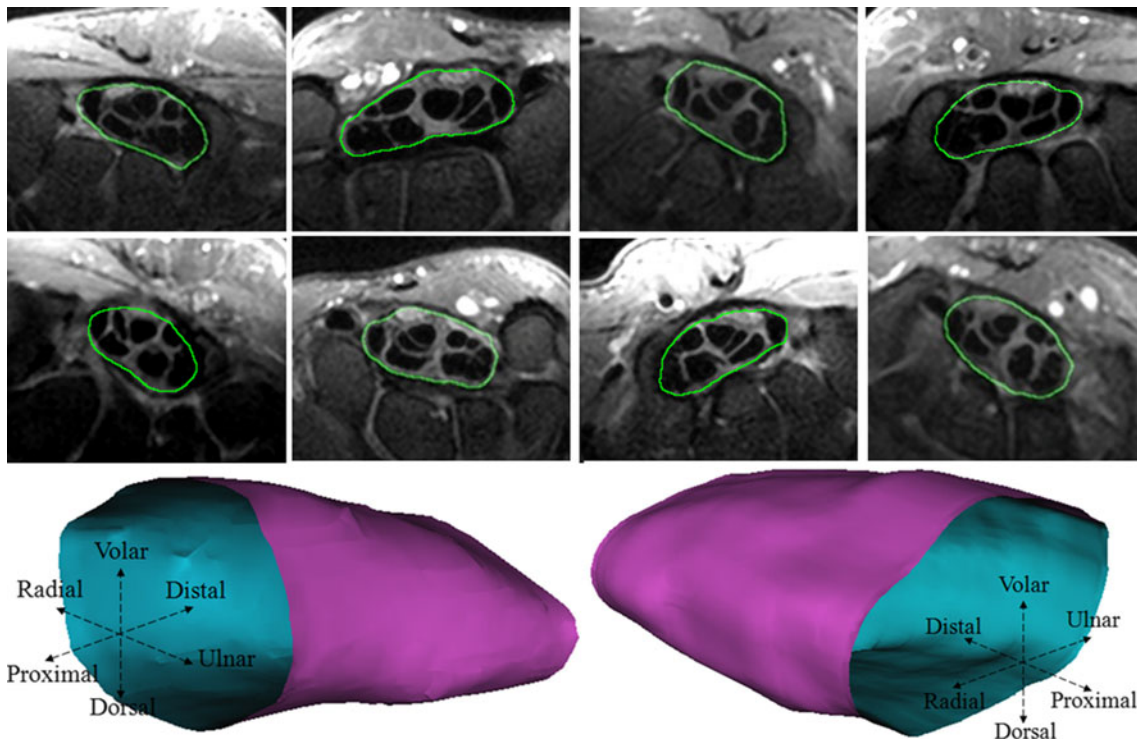


**Fig. 5** Segmentation results for the carpal tunnel by the proposed method: *first and second rows* the resulting contours superimposed onto axial PD-weighted MR images; *third row* the reconstructed

surfaces of the segmented tunnels, of which the first and second columns represent the carpal tunnels of two subjects

of the automatic result. A higher value of DSC and a smaller value of either ME or RMSE indicate better consistency between the automatic result and the ground truth. The evaluation results are reported in Table 1, of which each row lists the means and standard deviations of the DSC, ME, and RMSE from the axial images of each subject. The average DSC, ME, and RMSE were  $94.681 \pm 1.093$  %,  $0.294 \pm 0.067$  mm, and  $0.416 \pm 0.095$  mm, respectively.

**Comparative Study**

In this section, a comparative study was carried out to show the improvement of the proposed method over conventional methods on the automatic segmentation of carpal tunnel. To our knowledge, there have been no solutions proposed for carpal tunnel segmentation other than the proposed method. Therefore, two popular deformable model-based methods, the conventional snake [19] and the Chan–Vese method [33], were selected for comparison.

For the conventional snake, it is firstly considered that an initial contour is required for snake deformation on each image slice. To obtain a fair comparison, we adopted the same initial contour for snake as the proposed method did. Then, the snake was deformed toward the tunnel boundary on the most proximally cross-sectional image. After that, we adopted the same strategy on the rest cross-sectional images as the proposed sequential contour propagation (i.e., ICP-

based registration) did. Different from the proposed method, the conventional snake does not refer the intensity information on T1-weighted images (i.e., intensity transform function  $\varphi$  in Eq. 2) and does not utilize the geometric constraint of carpal tunnel and flexor tendons (i.e.,  $C_{geometry}$  in Eq. 4). As to the Chan–Vese method, which does not require an explicit initial contour, it can achieve segmentation by evolving an implicit curve (i.e., zero-level) based on the deduction of Euler–Lagrange equation [33]. Overall, the parameters of the Chan–Vese and conventional snake methods were selected empirically to obtain the best results.

The comparison was first achieved by visually evaluating the segmentation results obtained by both the proposed method and the other two methods. The two compared methods do not incorporate any anatomical knowledge and intensity characteristics of carpal tunnel from interprotocol MR images in the segmentation processes. The two selected methods cannot well handle the segmentation of carpal tunnel images, which are usually with complex anatomical context and fuzzy boundaries, thus failing in many cases. Two examples are demonstrated in Fig. 6a and b, which are two MR images (PD-weighted). Figure 6c and d is the segmentation results of the conventional snake. Figure 6e and f shows the segmentation results of the Chan–Vese method. Lastly, Fig. 6g and h shows the segmentation results of the proposed method. To highlight the results, we further superimposed the results onto the corresponding T1 images (see Fig. 6i and j).

**Table 1** Means and standard deviations of the accuracy measures of the DSC, ME, and RMSE estimated from the axial MR images of 15 subjects

Subject	DSC (%)	ME (mm)	RMSE (mm)
Subject 1 (8)	96.829±0.660	0.179±0.044	0.269±0.059
Subject 2 (8)	93.402±1.488	0.337±0.077	0.449±0.103
Subject 3 (9)	94.122±1.064	0.319±0.054	0.419±0.064
Subject 4 (7)	93.671±1.136	0.326±0.071	0.451±0.104
Subject 5 (10)	94.828±0.996	0.294±0.056	0.407±0.085
Subject 6 (7)	95.542±0.789	0.253±0.054	0.353±0.054
Subject 7 (8)	93.776±1.145	0.338±0.072	0.488±0.107
Subject 8 (7)	94.572±0.761	0.301±0.057	0.439±0.081
Subject 9 (9)	94.930±1.016	0.325±0.069	0.452±0.091
Subject 10 (10)	93.855±1.284	0.303±0.063	0.414±0.084
Subject 11 (10)	93.396±1.135	0.351±0.073	0.483±0.132
Subject 12 (10)	95.081±1.219	0.271±0.068	0.402±0.102
Subject 13 (8)	94.809±1.506	0.315±0.109	0.469±0.160
Subject 14 (7)	95.639±1.036	0.248±0.068	0.360±0.087
Subject 15 (8)	95.756±1.155	0.245±0.066	0.389±0.114
Mean±standard deviation	94.681±1.093	0.294±0.067	0.416±0.095

Number within parentheses represent the number of axial images covering the carpal tunnel.

Beyond the visual evaluation, we further carried out the quantitative comparison based on the measures of DSC, ME, and RMSE. Since using the Chan–Vese method obtains not only the contour of carpal tunnel but several contours of irrelevant anatomical structures, an objective quantitative comparison is difficult to perform. The quantitative comparison was only performed on the conventional snake and the proposed method. The evaluation results for the two examples obtained using the conventional snake were (84.558, 0.730, and 0.922) and (82.163, 1.048, and 1.375) in DSC (%), ME (mm), and RMSE (mm). The results obtained by

the proposed method were (95.188, 0.234, and 0.335) and (95.051, 0.248, and 0.300).

## Discussion

The images in this study naturally suffer from anatomical variability, including the size, position, and shape of carpal tunnel and its neighboring contexts (including tendons and fatty tissues). Moreover, as the images were taken at different time and from different subjects, there exist various

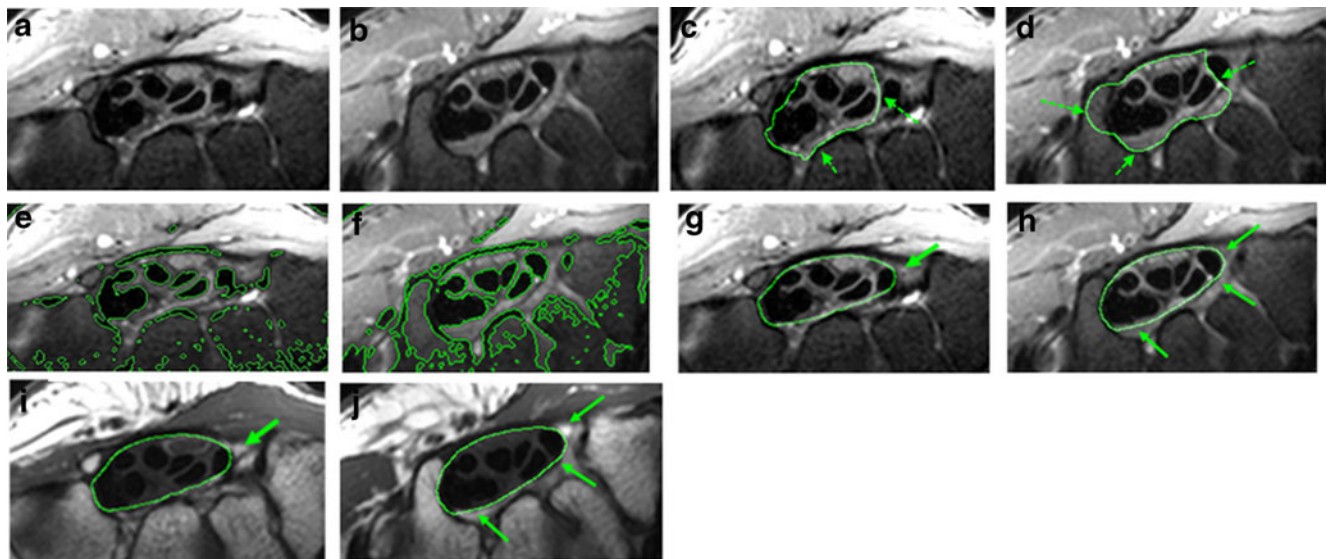


**Fig. 6** Comparison study: **a, b** the original images (PD-weighted); **c, d** the results of conventional snake; **e, f** the results of Chan–Vese method; **g, h** and **i, j** the results of the proposed method superimposed onto the PD-weighted and T1-weighted images, respectively

imaging conditions potentially affecting the image qualities, e.g., different coil position and distance to the wrist. Accordingly, these variations certainly lead to the anatomical and image noises embedded in the 15 cases of subject image data. As shown in the first and second rows in Fig. 5, desirable segmentation results that are very close to the true tunnel boundaries in the validation data can be obtained using the proposed method. Moreover, the resulting tunnel surfaces (the third row in Fig. 5) give realistic shapes and smooth surfaces as the true anatomical appearance of the carpal tunnel does. As for the quantitative evaluation, the average DSC was higher than 0.9, indicating a great overlap between the automatic and manual segmentation results [32]. Moreover, the average ME and RMSE were  $<0.5$  mm, which is very small compared to the average carpal tunnel width (about 20 mm). Furthermore, the small standard deviations in these accuracy measures indicate that the proposed method provides satisfactory reliability for carpal tunnel segmentation. From the accuracy evaluation for the fifteen subjects' data (large DSC, small ME, and RMSE), it was found that the proposed method can accommodate the effects of anatomical and image noises. The evaluation results are considered satisfactory for the requirements of biomechanical investigation and clinical studies of CTS.

In the comparison study, the conventional snake does not consider the geometrical relationship between the carpal tunnel and the flexor tendons, and intensity characteristics of carpal tunnel from interprotocol MR images, so the deformation is easily influenced by undesirable strong edges, as indicated by the dash arrows. Even though the snake was given initial models close to the true tunnel (same as the proposed method adopted), incorrect convergence of the deformation (see Fig. 6c and d) still occurred. As for the Chan–Vese method, it yielded a large number of incorrect and fragmentary regions, as shown in Fig. 6e and f. This is probably because the Chan–Vese method segments regions only based on homogeneity of image intensity, and it is thus difficult to differentiate tissues such as the flexor tendons, carpal bones, and transverse carpal ligament, which have similar intensities.

Compared to the results of the conventional snake and Chan–Vese methods, ours are more desirable because they have more realistic tunnel shapes and fit better with the true tunnel boundaries in the images, as indicated by the solid arrows in Fig. 6g and h. For each subject, the proposed method can automatically obtain an approximate subject-specific tunnel model based on the structural information of anatomical features, thus facilitating the convergence of the final segmentation process. In addition, anatomical knowledge was employed to define constraints to avoid some undesirable solutions (e.g., intersection of the tunnel boundary and flexor tendon boundaries). As a result, the proposed

method successfully overcame the difficulties of segmentation in MR carpal tunnel images (e.g., vague boundaries and confusing edges of irrelevant tissues) and obtained better segmentation results.

When evaluating the accuracy of an image segmentation method, the observer variability that potentially affects the reliability of the ground truth is usually a concern. An additional experiment, not demonstrated in this paper, found that the manual detection of tunnel boundary can be performed precisely by referring to both T1- and PD-weighted MR images. This experiment of manual detection by four experts obtained small interobserver variability with small standard deviations of DSC, ME, and RMSE (0.771, 0.044, and 0.038). As a result, the ground truth has not suffered from the interobserver variability in this case of carpal tunnel segmentation.

## Conclusions

Carpal tunnel segmentation in MR images is an essential requirement for investigating the causes and pathologies of CTS. We have proposed a new method, combining feature detection, object segmentation, and anatomical knowledge, to automatically segment the carpal tunnel from MR images. For each subject, a DM, which was well matched to the most proximally cross-sectional image, was automatically generated based on three anatomical features of the carpal tunnel. Moreover, both the T1 and PD image contents were utilized to calculate the edge energy in order to achieve precise segmentation of the carpal tunnel. Furthermore, the geometrical information obtained from the detected anatomical features was employed to constrain the shape deformation of the DM. Finally, we successfully achieved 3D segmentation of the carpal tunnel by sequentially propagating and evolving the segmented tunnel contour throughout the MR volume.

The accuracy of the proposed method was validated in both quantitative and qualitative experiments. The agreement between the automatic and manual segmentations was validated by a small margin of error and high spatial dependency. Moreover, the superior accuracy of the proposed method compared to the conventional methods was also demonstrated. In the future, the proposed method can be utilized to investigate the clinical signs of CTS for early diagnosis. It can also be extended to measure the structural changes of carpal tunnel in dynamic postures for the purpose of studying wrist kinematics.

**Acknowledgments** The authors would like to express their appreciation for the grant under contract NSC 99-2627-B-006-010 from the National Science Council, Taiwan, ROC. This work also utilized the shared facilities supported by the Medical Device Innovation Center, National Cheng Kung University, Tainan, Taiwan, ROC.

## References

1. Atroshi I, Gummesson C, Johnsson R, Ornstein E, Ranstam J, Rosén I: Prevalence of carpal tunnel syndrome in a general population. *JAMA* 282(2): 153–158, 1999
2. Thoma A, Veltri K, Haines T, Duku E: A meta-analysis of randomized controlled trials comparing endoscopic and open carpal tunnel decompression. *Plast Reconstr Surg* 114: 1137–1146, 2004
3. Tung WL, Zhao C, Yoshii Y, Su FC, An KN, Amadio PC: Comparative study of carpal tunnel compliance in the human, dog, rabbit, and rat. *J Orthop Res* 28: 652–656, 2010
4. Pacek CA, Tang J, Goitz RJ, Kaufmann RA, Li ZM: Morphological analysis of the carpal tunnel. *Hand* 5:77–81, 2010
5. Middleton WD, Kneeland JB, Kellman GM, Cates JD, Sanger JR, Jesmanowicz A, Froncisz W, Hyde JS: MR imaging of the carpal tunnel: normal anatomy and preliminary findings in the carpal tunnel syndrome. *Am J Roentgenol* 148: 307–316, 1987
6. Cudlip SA, Howe FA, Phil D, Clifton A, Schwartz MS, Bell BA: Magnetic resonance neurography studies of the median nerve before and after carpal tunnel decompression. *J Neurosurg* 96: 1046–1051, 2002
7. Ablove RH, Peimer CA, Diao E, Oliverio R, Kuhn JP: Morphologic changes following endoscopic and two-portal subcutaneous carpal tunnel release. *J Hand Surg* 19A: 821–826, 1994
8. Cobb TK, Bond JR, Cooney WP, Metcalf BJ: Assessment of the ratio of carpal contents to carpal tunnel volume in patients with carpal tunnel syndrome: a preliminary report. *J Hand Surg* 22A (4): 635–639, 1997
9. Uchiyama S, Itsubo T, Yasutomi T, Nakagawa H, Kamimura M, Kato H: Quantitative MRI of the wrist and nerve conduction studies in patients with idiopathic carpal tunnel syndrome. *J Neurol Neurosurg Psychiatry* 76: 1103–1108, 2005
10. Mogk JPM, Keir PJ: Evaluation of the carpal tunnel based on 3-D reconstruction from MRI. *J Biomech* 40: 2222–2229, 2007
11. Mogk JPM, Keir PJ: Wrist and carpal tunnel size and shape measurements: effects of posture. *Clin Biomech* 23: 1112–1120, 2008
12. Lluch AL: Thickening of the synovium of the digital flexor tendons: cause or consequence of the carpal tunnel syndrome? *J Hand Surg Br* 17(2): 209–212, 1992
13. Ham SJ, Kolkman WF, Heeres J, den Boer JA: Changes in the carpal tunnel due to action of the flexor tendons: visualization with magnetic resonance imaging. *J Hand Surg Am* 21(6): 997–1003, 1996
14. Moriya T, Zhao C, Cha SS, Schmelzer JD, Low PA, An KN, Amadio PC: Tendon injury produces changes in SSCT and nerve physiology similar to carpal tunnel syndrome in an in vivo rabbit model. *Hand* 6(4): 399–407, 2011
15. Kunze NM, Goetz JE, Thedens DR, Baer TE, Lawler EA, Brown TD: Individual flexor tendon identification within the carpal tunnel: a semi-automated analysis method for serial cross-section magnetic resonance images. *Orthop Res Rev* 1: 31–42, 2009
16. Xu S, Liu H, Song E: Marker-controlled watershed for lesion segmentation in mammograms. *J Digit Imaging* 24:754–763,2011
17. Nunzio GD, Tommasi E, Agrusti A, Cataldo R, Mitri ID, Favetta M, Maglio S, Massafra A, Quarta M, Torsello M, Zecca I, Bellotti R, Tangaro S, Calvini P, Camarlinghi N, Falaschi F, Cerello P, Oliva P: Automatic lung segmentation in CT images with accurate handling of the hilar region. *J Digital Imaging* 24(1): 11–27, 2011
18. Umesh Adiga PS, Chaudhuri BB: An efficient method based on watershed and rule-based merging for segmentation of 3-D histopathological images. *Pattern Recognit* 34: 1449–1458, 2004
19. Kass M, Witkin A, Terzopoulos D: Snake: active contour models. *Int J Comput Vis* 1(4): 321–331, 1988
20. Rangayyan RM, Kamenetsky I, Benediktsson H: Segmentation and analysis of the glomerular basement membrane in renal biopsy samples using active contours: a pilot Study. *J Digit Imaging* 23 (3): 323–331, 2010
21. Cootes TF, Taylor CJ, Cooper DH, Graham J: Active shape models-their training and application. *Comput Vis Image Underst* 61(1): 38–59, 1995
22. Snel JG, Venema HW, Grimbergen CA: Detection of the carpal bone contours from 3D MR images of the wrist using a planar radial scale-space snake. *IEEE Trans Med Imaging* 17(6): 1063–1072, 1998
23. Santarelli MF, Positano V, Michelassi C, Lombardi M, Landini L: Automated cardiac MR image segmentation: theory and measurement evaluation. *Med Eng Phys* 25: 149–159, 2003
24. Han CC, Lee CH, Peng WL: Hand radiograph image segmentation using a coarse-to-fine strategy. *Pattern Recognit* 40: 2994–3004, 2007
25. Seifert S, Wächter I, Schmelzle G, Dillmann R: A knowledge-based approach to soft tissue reconstruction of the cervical spine. *IEEE Trans Med Imaging* 28(4) : 494–507, 2009
26. Yu J, Wang Y., Chen P: Fetal ultrasound image segmentation system and its use in fetal weight estimation. *Med Bio Eng Comput* 46: 1227–1237, 2008
27. Zhang TY, Suen CY: A fast parallel algorithm for thinning digital patterns. *Communications of the ACM* 27(3): 236–239, 1984
28. Chen HC, Sun YN, Wang YY, Lin CH, Wang CK, Jou IM: Segmentation of flexor tendons within carpal tunnel from magnetic resonance image. In: *International Computer Symposium (ICS)*, Tainan, Taiwan, 2010, pp 932–935
29. Dhawan AP: *Medical Image Analysis*. Hoboken: Wiley-Interscience, 2003, pp 186–187
30. Besl PJ, McKay ND: A method for registration of 3-D shapes. *IEEE Trans Pattern Anal Mach Intell* 14(2): 236–256, 1992
31. Lorensen WE, Cline HE: Marching cubes: A high resolution 3-D surface construction algorithm. *Comput Graph (ACM SIG)* 21(4): 163–169, 1987
32. Zou KH, Warfield SK, Bharatha A, Tempany CM, Kaus MR, Haker SJ, Wells WM, Jolesz FA, Kikinis R: Statistical validation image segmentation quality based on a spatial overlap index. *Acad Radiol* 11: 178–189, 2004
33. Chan TF, Vese LA: Active contour without edges. *IEEE Trans Image Process* 10 (2): 266–277, 2001